

TRANSITION FLIGHT ANALYSIS OF AN AGILE UNMANNED AIR VEHICLE

Adnan Maqsood, Tiau Hiong Go

**School of Mechanical and Aerospace Engineering, Nanyang Technological University,
Singapore 639798, Republic of Singapore**

Keywords: UAV, transition, trajectory optimization, flight dynamics

Abstract

The paper discusses hover-to-cruise transition maneuver performance of a small UAV designed for operations in confined spaces and cluttered terrains. The objective of the study is to achieve a transition scheme with minimal variation in altitude, reduced transition time and reasonable thrust-to-weight ratio. For this purpose, the conventional fixed-wing platform is compared with the modified platform having variable-incidence wing referred as 'aerodynamic-vectoring'. The effects of aerodynamic vectoring are discussed in comparison with the conventional configuration based on altitude loss, transition time, thrust-to-weight ratio required and the control efforts. A parametric study encompassing the effects of mass and aspect ratio is incorporated to evaluate the design requirements for the platforms. The linearized dynamic analysis in longitudinal plane across the complete transition maneuver is carried out for both configurations. The results indicate that the advantage of the aerodynamic vectoring increases with the increase in mass and aspect ratio. Moreover the variable-incidence wing can reduce the maximum thrust-to-weight ratio requirement as well as elevator control efforts. Short-period and phugoid mode are also compared.

1 Introduction

Recently, there is a significant shift in design paradigm for Mini-Unmanned Air Vehicles (UAV). Present and future generation UAVs are expected to undergo agile maneuvers in an effort to enlarge the mission envelope. The

operational demands to perform missions indoor and outdoor can only be achieved by increasing platform versatility. Typical mission attributes for such vehicles include vertical take-off and landing (VTOL), hover, cruise flight and increased maneuverability in confined spaces. Such efforts lead to a type of baseline aircraft design that can perform hover coupled with efficient forward flight [1] commonly known as 'convertible' platforms. Green [2, 3] has met such operational demands on fixed-wing platform by doing prop-hanging with excessively high thrust-to-weight ratios and transitioning between hover and cruise. These transition maneuvers pose significant challenges to designers. These challenges include significant altitude variation, loss of partial control and high thrust-to-weight ratio designs. During the earlier studies by [4], such convertible platforms have been discussed and emphasis is made on introducing variable-incidence wing to increase platform versatility in executing such mission profiles.

During recent studies[5, 6], significant efforts have been made on the techniques to broaden the flight envelope and [7, 8] have carried out detailed studies on characteristics associated with transition maneuvers. Kubo[9] has introduced utilization of slats and flaps for efficient transitions but thrust-to-weight ratio is yet to be addressed. Stability of such mission segments is an important issue which has not been widely covered in literature.

In this work a novel scheme named as 'aerodynamic vectoring' is introduced such that the angle of incidence of the wing is dealt as a control variable. It is also referred as the variable-incidence wing feature. The optimal trajectory analysis is carried out to estimate the

hover-to-cruise transition performance. The comparative study with the conventional design is carried throughout the paper. In order to study the stability characteristics, linearized flight dynamic analysis in longitudinal mode is studied and discussed as well. The aerodynamic forces and moments database is developed both in pre-stall and post-stall regime using a 3-dimensional vortex lattice code.

2 Aircraft Modeling

In this section, the geometry of the aircraft is described and is followed by its aerodynamic evaluation across the whole maneuver range. During the low speed flight, control is fundamentally driven from elevator submerged in the slipstream of the propeller. The propulsive effects are also discussed in this section.

2.1 Geometry of the Aircraft

The geometric configuration of the aircraft under study is shown in Fig. 1. The aircraft is a conventional wing-tail configuration with a tractor-type propulsion system. The aircraft has got a maximum box wise dimension of 1 m. The dimensional scales of the model include a rectangular wing, a propeller diameter of 0.254 m, and a mean aerodynamic chord of 0.2379 m. The wing and tail comprise of NACA 0012 airfoil. The study incorporates the phenomena of aerodynamic vectoring therefore, it can be seen that the outboard section is decoupled and free to rotate. The complete wing is divided into two sections: inboard and outboard sections. The inboard section (0.25 m span) is fixed with the fuselage and it is submerged in the slipstream of the propeller. The outboard section, on the other hand, can be rotated about its quarter-chord axis (called variable-incidence wing or aerodynamic vectored configuration).

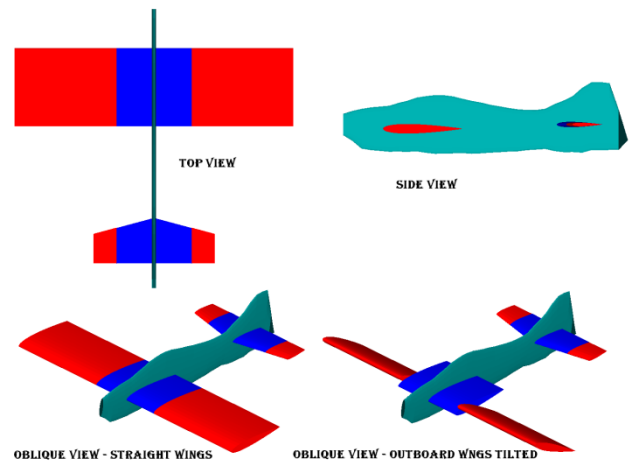


Fig. 1. Geometric Views of the UAV

The study also incorporates the effect of aspect ratio on the performance analysis of the transition maneuver. Therefore, for studying an alternate configuration having different aspect ratio, the outboard wings are cropped such that the aspect ratio is reduced to 2.5. The planform views of original and cropped configurations are shown in Fig. 2. The areas under the slipstream are colored blue and free-stream areas are narrated by red.

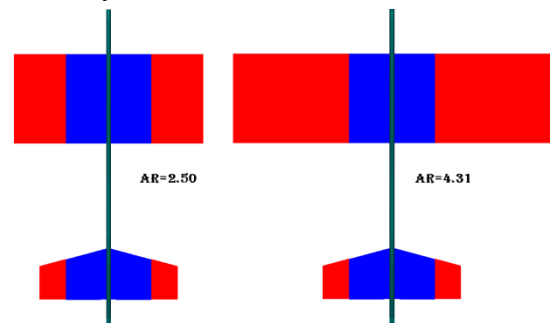


Fig. 2. Planform views of the two variants from the top

2.2 Aerodynamic Estimation

The aerodynamics of the aircraft is computed using a commercial code called MultiSurface Aerodynamics (MSA)[10]. MSA is based on 3 Dimensional Vortex Lattice Method (VLM3D), a well-established technique based on panel methods, which is derived from potential flow theory and provides inviscid aerodynamic calculations (e.g. see [11] for further details). Using the effective angles of attack along the wing span as computed using

VLM and utilizing the boundary layer theory, the total profile drag can be calculated by integrating the incremental profile drag at various span locations. For the evaluation of the aerodynamic properties in the post-stall regime, the numerical code works using the same boundary layer approximation technique for the calculation of the transition and separation points.

The aerodynamics is integrated on component-buildup technique such that the aerodynamic contribution from inboard wing, fuselage, rudder and inboard horizontal tail are submerged under slipstream effects whereas; the outboard wings and horizontal tail are under free-stream effects. For the slip-stream evaluation, [12] formulation for free propellers based on Glauert's hypothesis is used. The induced velocity aft of the propeller is a function of the free-stream velocity, angle of attack on the propeller, altitude and disc area.

$$w^4 + 2V(\cos\alpha)w^3 + V^2w^2 = \left(\frac{T}{2\rho A}\right)^2 \quad (1)$$

where w is the induced velocity and A is the disc area of the propeller. Now the aerodynamic properties of the UAV are discussed. The aerodynamic lift and drag forces are plotted in Fig. 3 and 4 respectively. It should be noted that the forces are plotted at several velocities such that there are no propulsion effects. Moreover, conventional wing configuration is considered. In Fig. 3, lift is plotted against the angle of attack from 0° to 90° at several velocities. It is evident from the figure, that the low aspect ratio wings of 2.5 has significantly delayed stall to that of aspect ratio of 4.31. Moreover, the pre-stall lift curve slope possesses slight non-linearity compared to that of AR=4.31 as the results are obvious from aircraft configuration aerodynamics. The variation of drag with angle of attack is plotted across several velocities in Fig. 4. The conventional behavior of the increase in drag due to the increase in velocity and angle of attack is observed for both cases. Moreover, with the increase in aspect ratio, the surface area increases and thereby, significant increase in

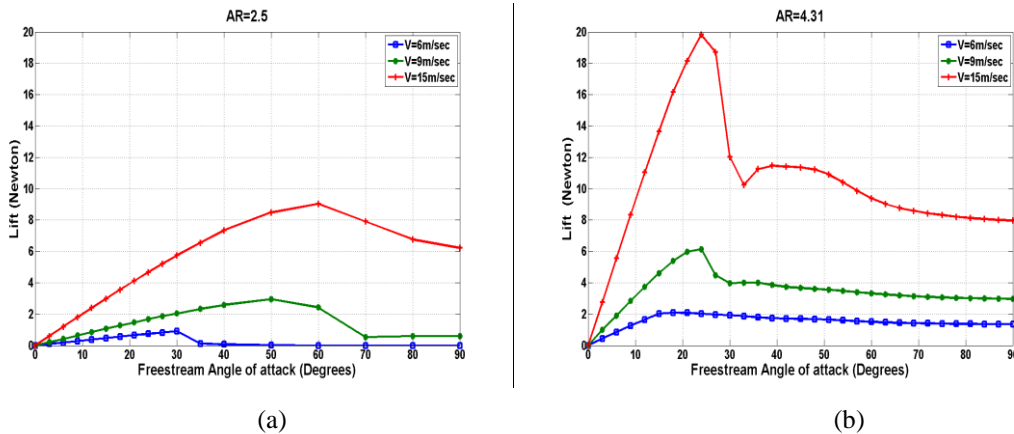


Fig. 3. Lift plot from 0° to 90° at several velocities. AR=2.50(a) and AR=4.31(b)

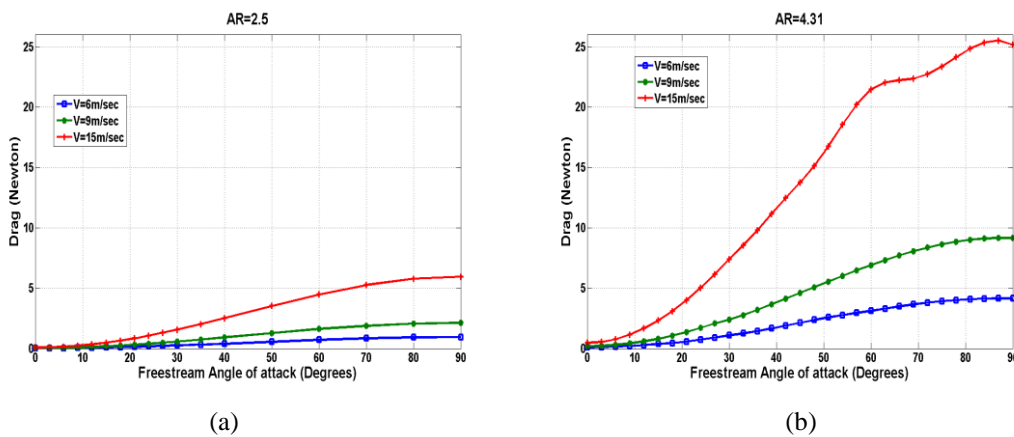


Fig. 4. Drag plot from 0° to 90° at several velocities. AR=2.50(a) and AR=4.31(b)

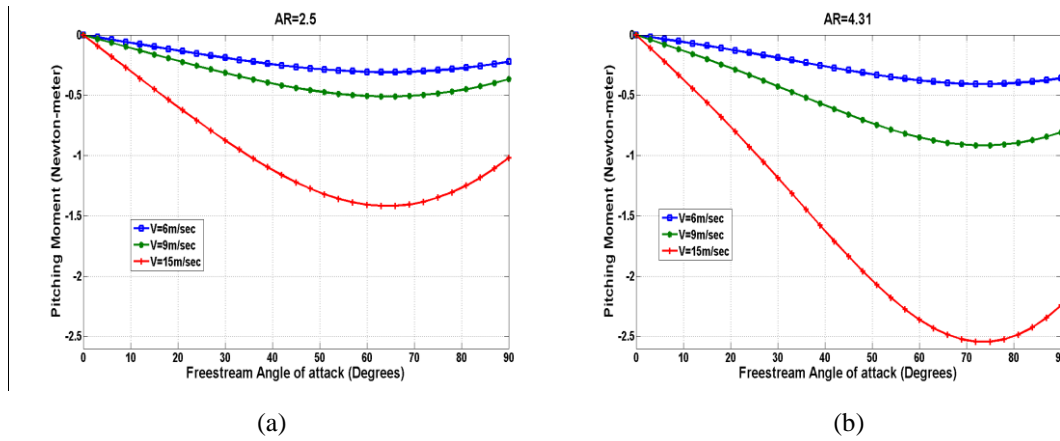


Fig. 5. Pitching Moment plot from 0^0 to 90^0 at several velocities. AR=2.50(a) and AR=4.31(b)

pressure and viscous forces is observed for the AR=4.31 configuration. The centre of gravity of the aircraft is fixed at 20 cm aft of the nose for both cases. The high AR wing configuration is more stable longitudinally than the low AR case over the range of angle of attack as shown in Fig. 5 because of the higher static pitching moment slope. The pitch stability is greatly affected by the location of the centre of pressure over the lifting surfaces. The centre of pressure generally shifts backward with the increase in angle of attack. For the low AR wing, a higher percentage of planform area comes under the influence of wing tip vortices than the high AR one. As the angle of attack increases, the wing tip vortices move the centre of pressure downstream.

3 Trajectory Optimization

In this section optimal transition trajectories of varying thrust-to-weight ratios, mass of the aircraft and aspect ratio of the wing are discussed explicitly. Additionally, the transition maneuver performances are compared between the conventional fixed-wing configuration (two control variables: thrust and elevator deflection) and the proposed aerodynamic vectored variable-incidence wing (three control variables: thrust, elevator deflection and angle of incidence of outboard wing).

The vehicle dynamics is formulated as a two-degree of freedom point mass model with pitching constraints and thus the dynamics discussed here is restricted in longitudinal plane. The assumption is valid in the absence of out-of-plane forces and moments. Thus, this study does not cover the effects of wind disturbances

and asymmetries in the aircraft layout. These assumptions simplify the aerodynamics and vehicle dynamics substantially while still providing qualitative as well as quantitative insight to the hover-to-cruise transition properties.

3.1 Problem Formulation

3.1.1 Governing Dynamics

To analyze the variety of flight conditions ranging from hover to forward flight state, the following equations of motion, which are similar to the ones used in earlier pilot study [4], are used.

$$m\ddot{x} = T \cos \alpha_D - D - W \sin \gamma \quad (2)$$

$$m\ddot{z} = L + T \sin \alpha_D - W \cos \gamma \quad (3)$$

where m is the mass of the aircraft, \ddot{x} is the absolute acceleration aligned with horizontal direction, \ddot{z} is the absolute acceleration aligned with vertical direction, $W = mg$ is the weight of the aircraft and T is the thrust. L and D represent aerodynamic lift and drag respectively. γ is the flight path angle of the aircraft.

3.3.1 Optimization Algorithm

The optimal trajectory calculation is based on a fixed-time two point boundary value problem between the hover and the forward flight states. The optimal trajectories are evaluated using commercial nonlinear constrained programming algorithm *fmincon* available in MATLAB optimization toolbox. The algorithm is based on a sequential quadratic programming technique coupled with Quasi-Newton method for better efficiency. The sampling time between two consecutive control inputs is 0.2 seconds. The control variables for

the optimization are α_{fus} , α_{wing} and T , as follows:

$$\vec{u} = (\alpha_{fus} \quad \alpha_{wing} \quad T)^T \quad (4)$$

For the conventional case, the same control vector can be used by imposing an additional constraint that at any instant:

$$\alpha_{fus} = \alpha_{wing} \quad (5)$$

The objective function for the optimization is based on kinetic and potential energy formulation such that:

$$J = w_1 \cdot \frac{1}{2} m |(u_t)^2 - (15)^2| + w_2 \cdot \frac{1}{2} m v_t^2 + w_3 \cdot \left(\sum_{i=1}^t |y_i| \right) \quad (6)$$

The first term in the objective function (6) indicates the difference in the kinetic energy due to the terminal horizontal velocity and the target horizontal cruise velocity, which is 15 m/sec. The second term in (6) represents the kinetic energy due to terminal vertical velocity and the third term represents the potential energy. The weighting factors (w_1 , w_2 and w_3) can be adjusted to achieve the desired performance. In this study, the weighting factors used are: $w_1 = w_2 = w_3 = 1$, the same for both fixed and variable-incidence wing cases. The common constraints applied to the dynamics of the vehicle during hover-to-cruise optimization for both cases are shown in Table 1.

$V \geq 0$	$u_i \geq 0$	$u_i \leq 15m/s$
$\alpha_{fus} \geq 0$	$\alpha_{fus} \leq \frac{\pi}{2}$	$\Delta\alpha_{fus} \leq 10^\circ / step$
$\alpha_{wing} \geq 0$	$\alpha_{wing} \leq \frac{\pi}{2}$	$\Delta\alpha_{wing} \leq 10^\circ / step$
$T_i \geq 0.5$	$T_i \leq T_{max}$	$\Delta T \leq 2N / step$
$\dot{\alpha}_{fus} \leq 50^\circ / s$	$\dot{\alpha}_{wing} \leq 50^\circ / s$	$\dot{T} \leq 4N / s$

Table 1 Constraints used in trajectory optimization

where V is the freestream velocity, u_i is the horizontal velocity at i^{th} instant, α_{fus} is the angle of attack of the aircraft, α_{wing} is the angle of attack of the outboard wing section, T_i is the thrust produced by the propeller at i^{th} instant. The angular rate constraints are included in order to capture the pitching rate limitations so

that the real aircraft dynamics are better represented.

3.2 Trajectory Analysis

The trajectory analysis is carried out for different parameters like thrust-to-weight ratio, mass of the UAV and aspect ratio across several transition times. The emphasis is made to carry out constant altitude transition trajectories. A representative case of the likely optimized transition maneuver is given in Fig. 6 and 7, which shows the conventional (fixed-incidence) and aerodynamic vectored (variable-incidence) cases. The positions of aircraft are shown at several indicated time instants and velocities with approximate attitude of the aircraft and wing. It should be noted that during the optimized transition for aerodynamic vectoring case, the angle of incidence of the wing always remains in the vicinity of pre-stall regime. This shows the optimized aerodynamic-assistance to the aircraft transition dynamics. It should also be noted that the constant altitude transitions can also be achieved in the fixed-incidence case (Fig. 6) but with a higher T/W .

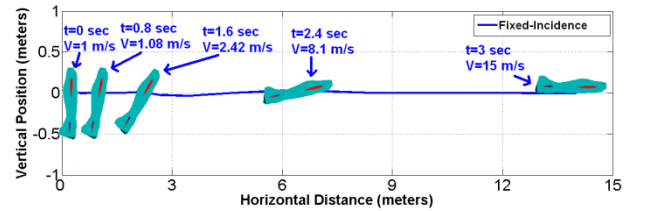


Fig. 6. Generic transition trajectory without aerodynamic vectoring

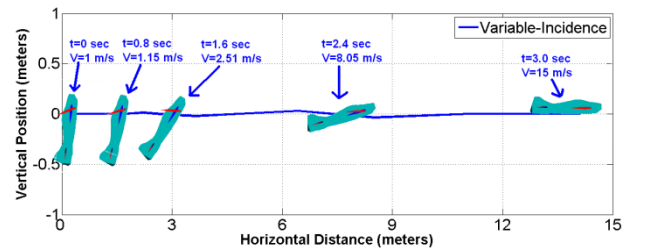


Fig. 7. Generic transition trajectory with aerodynamic vectoring

3.2.1 Effect of Mass

Now, the effect of aerodynamic vectoring on the required $(T/W)_{max}$ to perform a

hover-to-cruise transition with no loss of altitude is analyzed. In Fig. 8, the required $(T/W)_{max}$ for the constant altitude transitions is plotted across several mass for conventional and aerodynamic vectoring cases. It is observed that the increase in mass of the UAV increases the $(T/W)_{max}$ requirement for a particular transition time. Moreover, the increase in transition time reduces the $(T/W)_{max}$ requirement. The trend is similar for different mass values. It is also observed that with the use of the variable-incidence wing, the dependency on $(T/W)_{max}$ is significantly reduced especially for the shorter transition times. As longer transition time is allocated, the advantage of the variable-incidence wing becomes less obvious. For the application of indoor autonomous UAVs, shorter time is very desirable and with the substantial decrease in $(T/W)_{max}$ requirement for a particular mass, the variable-incidence wing feature offers a significant advantage.

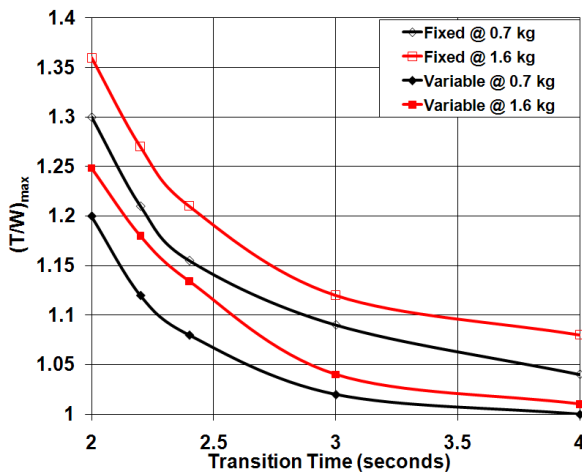


Fig. 8. Effect of mass on $(T/W)_{max}$ on transition performance with and without aerodynamic vectoring

3.2.2 Effect of Aspect Ratio

Since size is a primary constraint for UAVs designed for application in a confined space therefore the inherent attribute of such vehicles is the low aspect ratio wing design. For this reason, the effect of the aspect ratio on the hover-to-cruise transition performance is examined here. As discussed in the aerodynamic section, two configurations having AR of 4.31 and 2.50 are compared. The results shown in this section are associated with mass of 0.7 kg for brevity purposes.

In Fig. 9, the $(T/W)_{max}$ needed for various transition times are plotted for the two aspect ratios considered for both conventional and aerodynamic vectored cases. As obvious from all the scenarios simulated, the increase in the transition maneuver time reduces the required $(T/W)_{max}$. For the fixed-wing case, the thrust-to-weight ratio requirement increases by approximately six percent with the decrease in aspect ratio from 4.31 to 2.50. The reason for this is with the decrease in the planform area of the wing, the contribution of the aerodynamic forces is less significant and the transition maneuver becomes dominated by the propulsive force. Another advantage of the variable-incidence wing can also be seen in Fig. 9. Even at the low aspect ratio of 2.50, the use of the variable-incidence wing leads to the lower requirement on $(T/W)_{max}$ when compared to the fixed-wing case of the same aspect ratio.

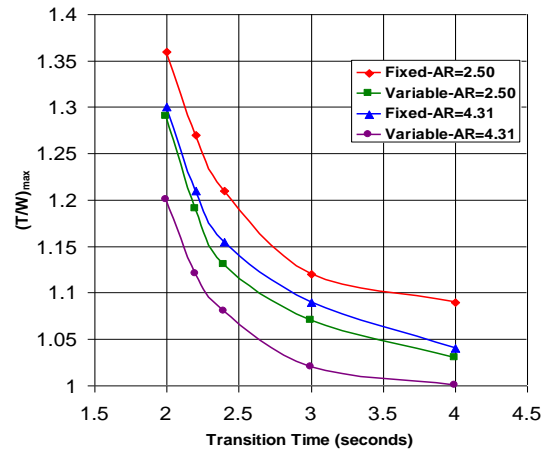


Fig. 9. Effect of AR on transition performance with and without aerodynamic vectoring

4 Longitudinal Flight Dynamic Analysis

After getting the optimal trajectories from point mass model, the next aim is to study the UAV dynamic responses and its stability. In this section, the longitudinal dynamics of the agile UAV equipped with the aerodynamic vectoring feature is discussed. The conventional non-linear equations of motion are linearized based on small disturbance theory [13]. The trim points are evaluated across the vehicle's velocity range. The stability derivatives are evaluated from the aerodynamic results discussed previously as well as from some

empirical techniques. The dynamic stability is analyzed across several trim points to examine the possible change in stability characteristics.

4.1 Problem Formulation

4.1.1 Linear Dynamics

The nonlinear longitudinal dynamic equations can be represented as below.

$$\begin{aligned} \dot{u} &= \frac{X}{m} - g \sin \theta - qw \\ \dot{w} &= \frac{Z}{m} + g \cos \theta + uq \\ M &= I_{yy} \dot{q} \end{aligned} \quad (7)$$

where u, w are horizontal and vertical velocities respectively; X and Z are the horizontal and vertical force vectors; M is the pitching moment; g is the acceleration due to gravity; q is the pitch rate; m is the mass of the aircraft and I_{yy} is the moment of inertia in the longitudinal mode.

The nonlinear equations of aircraft motion are linearized about a specific trim point with the aid of small disturbance theory. Eq. (8) shows the linearized longitudinal equations in state-space form proposed by [13] with a few additional stability derivatives.

$$\begin{bmatrix} m & 0 & 0 & 0 \\ 0 & m - \hat{Z}_{\dot{w}} & 0 & 0 \\ 0 & -\hat{M}_{\dot{w}} & I_{yy} & 0 \\ 0 & 0 & 0 & 1 \end{bmatrix} \begin{bmatrix} \dot{u} \\ \dot{w} \\ \dot{q} \\ \dot{\theta} \end{bmatrix} = \begin{bmatrix} \hat{X}_u & \hat{X}_w & 0 & -mg \cos \Theta_0 \\ \hat{Z}_u & \hat{Z}_w & \hat{Z}_q + mU_0 & -mg \sin \Theta_0 \\ \hat{M}_u & \hat{M}_w & \hat{M}_q & 0 \\ 0 & 0 & 1 & 0 \end{bmatrix} \begin{bmatrix} u \\ w \\ q \\ \theta \end{bmatrix} + \begin{bmatrix} \Delta X^c \\ \Delta Z^c \\ \Delta M^c \\ 0 \end{bmatrix} \quad (8)$$

Where the last vector is the control parameter. If we present stability derivatives by dividing them with its moment of inertias/mass, such that $X_u = \hat{X}_u / m, Z_u = \hat{Z}_u / m$ and $M_q = \hat{M}_q / I_{yy}$ the comprehensive form of matrix A can be presented as

$$A = \begin{bmatrix} X_u & X_w & 0 & -g \cos \Theta_0 \\ \frac{Z_u}{1 - Z_{\dot{w}}} & \frac{Z_w}{1 - Z_{\dot{w}}} & \frac{Z_q + U_0}{1 - Z_{\dot{w}}} & \frac{-g \sin \Theta_0}{1 - Z_{\dot{w}}} \\ M_u + Z_u \Gamma & M_w + Z_w \Gamma & M_q + (Z_q + U_0) \Gamma & -g \sin \Theta_0 \Gamma \\ 0 & 0 & 1 & 0 \end{bmatrix} \quad (9)$$

where $\Gamma = \frac{M_{\dot{w}}}{1 - Z_{\dot{w}}}$. In the next section,

the trim states are evaluated for the variable incidence wing configuration and the dynamic stability approximations are carried out to evaluate the UAV dynamics.

4.1.2 Trim Analysis

The trim state comparison of the conventional configuration is carried out against the aerodynamic vectored UAV. The trim analysis is carried out by the optimization of cost function that incorporates translational forces plus rotational moment. The cost function is minimized by using MATLAB® routine *fmincon* based on non-linear SQP method and Quasi-Newton methods similar to section 3. The forces and moment involved may be represented in the following manner:

$$\begin{aligned} X &= X_{Aero} + X_{Thrust} + X_{Grav} + X_{Other} \\ Z &= Z_{Aero} + Z_{Thrust} + Z_{Grav} + Z_{Other} \\ M &= M_{Aero} + M_{Thrust} + M_{Other} \end{aligned} \quad (10)$$

where $(\cdot)_{Aero}, (\cdot)_{Prop}$ and $(\cdot)_{Grav}$ represents aerodynamic, propulsive, gravitational and miscellaneous contributions respectively. The control parameters to be optimized for the trim states from 0 to 15 m/sec velocity range are:

$$\vec{u} = (\alpha_{fus}; \alpha_{wing}; T/W; \delta_{elev})^T \quad (11)$$

where δ_{elev} is the elevator angle with respect to the fuselage. The cost function to be minimized in the optimization is as follows:

$$J = X^2 + Z^2 + M^2 \quad (12)$$

For trim flight conditions, the components of the resultant forces and moments X, Z and M must be in equilibrium state. X, Z and M represents the axial, vertical and pitch moment in the stability axis system. The constraints posed to the state variables are shown below.

$$\left\{ \begin{array}{l} 0^0 \leq \alpha_{fus} \leq 90^0 \\ 0^0 \leq \alpha_{wing} \leq 30^0 \text{ (Aerodynamic - Vectoring)} \\ \alpha_{fus} = \alpha_{wing} \text{ (Conventional)} \\ 0 \leq T/W \leq 1.00 \\ -20^0 \leq \delta_{elev} \leq 20^0 \end{array} \right. \quad (13)$$

We can have multiple sets of trim points based on different initial conditions. Based on careful selection, single trim states across different velocities are evaluated as shown in Figs. 9 to 13 for the conventional and aerodynamic vectoring cases. The biggest advantage as evident from Fig. 9 is in terms T/W requirement. The T/W requirement for the variable-incidence scheme is significantly lower than the fixed-incidence scheme over the greater transition range.

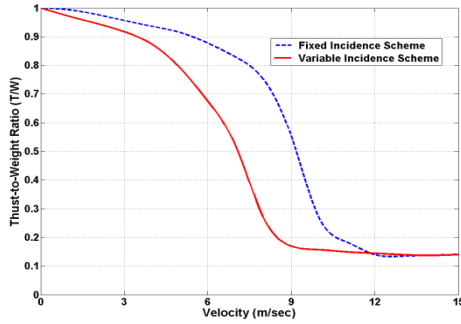


Fig. 10. Trim (T/W) with and without aerodynamic vectoring

In Fig. 11, the pitch attitude of the UAV reduces from 90^0 in hover to the cruise pitch angle as the velocity of the UAV increases for both cases. The shift from hover attitude to cruise attitude occurs once the aerodynamic effectiveness is improved to lift the aircraft.

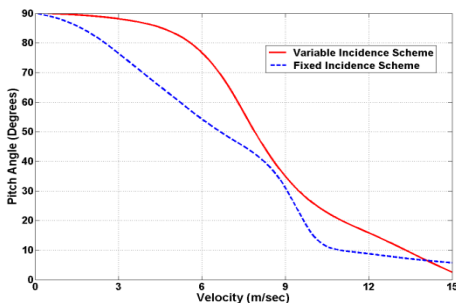


Fig. 11. Trim pitch angle with and without aerodynamic vectoring

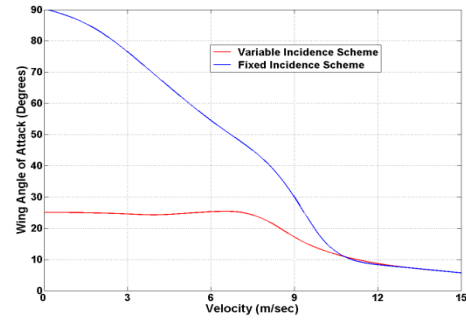


Fig. 12. Wing angle of attack with and without aerodynamic vectoring

In Fig. 12, for the aerodynamic vectored UAV the wings remain at Cl_{max} state before the transition speed of 7-8 m/sec. Note for fixed-wing case, α_{wing} remains aligned with α_{fus} .

As observed in Fig. 13, the elevator deflection for the fixed-wing scheme is higher than that of the variable-incidence wing one at low speeds, thereby reducing the elevator control authority to counter disturbances. From practical point of view, reduced elevator demands are desirable during slow speeds to have sufficient margin to cater for any disturbances.

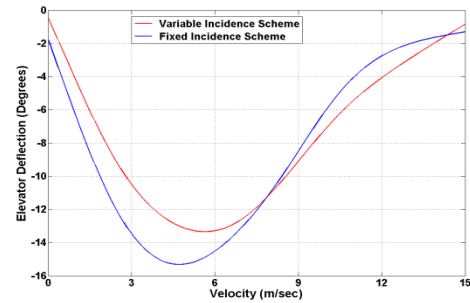


Fig. 13. Elevator deflection angle with and without aerodynamic vectoring

The steady-state trim analysis has shown significant advantages of aerodynamic vectored UAV over conventional UAV in terms of reduced T/W requirement and elevator deflection to achieve the trimmed states.

4.2 Analysis of Dynamic Characteristics

Based on the formulation of the section 4.1.1, the stability derivatives are evaluated at all velocities ranging from 1 m/sec to 15 m/sec around the trim points. Then the stability derivatives are used to evaluate eigenvalues

associated with the matrix A as shown in Eq. (9). The open-loop stick-fixed stability of the aircraft in its operational velocity range is evaluated. The dynamic stability characteristics of the aerodynamic vectoring case are compared with the fixed-incidence wing one.

In Figs. 14 and 15, the eigenvalues associated with the short period mode for various airspeeds are plotted for the conventional and aerodynamic vectored cases. At higher speeds (beyond 8 m/s), the short-period mode of both cases is stable and its damping increases with the increase in airspeed. For the variable-incidence wing case, the short period mode becomes unstable between 7 and 8 m/s speeds. Note however, that the current analysis is based on steady trim-point properties. It remains to be seen whether the instability exhibited by the variable-incidence wing case in the specific airspeed range is divergent or exhibits stable orbital stability in terms of limit-cycle oscillations.

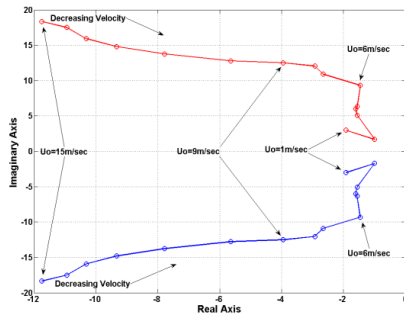


Fig. 14. Short-period eigenvalue migration without aerodynamic vectoring

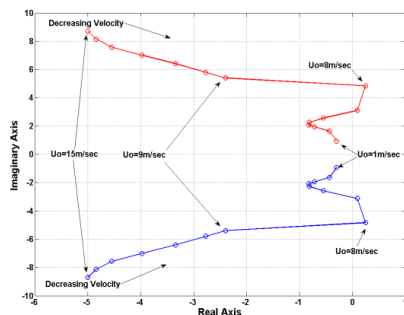


Fig. 15. Short-period eigenvalue migration with aerodynamic vectoring

In Figs. 16 and 17, the variations of the phugoid eigenvalues are plotted for both fixed and variable-incidence wing cases. The eigenvalues for the phugoid mode show subtle

behavior relative to short-period mode. The comparison of phugoid mode between the fixed and variable-incidence wing cases indicates that the variable-incidence wing aircraft has a reduced phugoid damping compared to the fixed-wing. The phugoid damping is affected by the lift to drag ratio as can be seen from the phugoid damping approximations below.

$$\zeta_{ph} = \frac{1}{\sqrt{2}} \frac{1}{L/D} \quad (14)$$

The higher the lift to drag ratio, the lower the damping will be. For the aerodynamic vectoring case, L/D is substantially higher because the wings remain in the pre-stall regime across all trimmed states, as shown in Fig. 12, whereas for the fixed-wing case, the wing stays in post-stall regime for the most trimmed conditions, especially at low speeds. This causes the reduction in L/D for the fixed-incidence case and therefore, its phugoid damping is relatively higher to that of the variable-incidence one. In general, phugoid instability is less of a concern compared to the short period one due to its relatively low frequency.

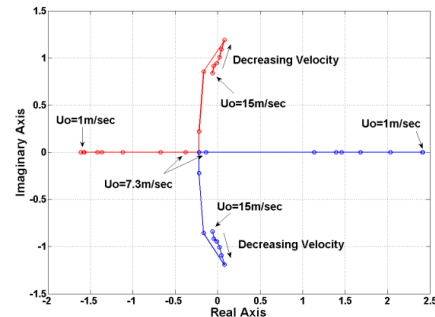


Fig. 16. Phugoid eigenvalue migration without aerodynamic vectoring

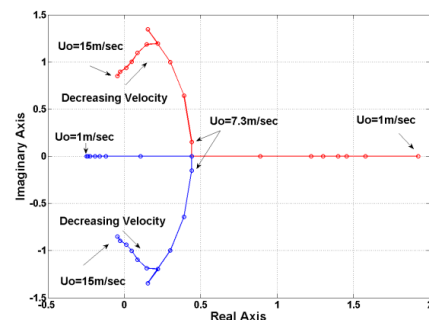


Fig. 17. Phugoid eigenvalue migration with aerodynamic vectoring

5 Conclusion and Future Work

An aerodynamic-vectoring phenomena is used to mitigate the problems associated with the transition maneuver for small unmanned air vehicles (UAV). The addition of the angle of incidence of the wing as a control variable has delivered promising results for improving hover-to-cruise transitions at reasonable thrust-to-weight ratios with minimum penalty on time and altitude loss. During the trajectory analysis, the effects of mass and aspect ratio are quantified. The optimal trajectories are generated for the analysis on the hover-to-cruise transition performance. Results indicate that the advantage of the variable-incidence wing scheme becomes more obvious with the increase in mass of the vehicle but becomes less obvious with the decrease in the wing aspect ratio. The maximum thrust-to-weight ratio and elevator requirement can also be reduced with aerodynamic vectoring. However, linear analysis indicates that the variable-incidence wing leads to short-period instability at certain airspeed range. Further investigation of the true nature of the dynamics is needed, especially in that airspeed range, to determine the proper control required to achieve the desired stable trimmed flights.

References

- [1] Pines, D.J. and F. Bohorquez, Challenges Facing Future Micro-Air-Vehicle Development. *Journal of Aircraft*, Vol. 43, No. 2, pp. 290-305 2006.
- [2] Green, W.E. and P.Y. Oh. *A MAV That Flies Like an Airplane and Hovers Like a Helicopter*. in *2005 IEEE/ASME International Conference on Advanced Intelligent Mechatronics*. Monterey, California, 2005.
- [3] Green, W.E. and P.Y. Oh. *Autonomous Hovering of a Fixed-Wing Micro Air Vehicle*. in *Proceedings 2006 IEEE International Conference on Robotics and Automation*, 2006.
- [4] Maqsood, A. and T.H. Go. *Study on Aerodynamic Assisted Transition Control Technique for Versatile UAV*. in *47th AIAA Aerospace Sciences Meeting*. Orlando, Florida, 2009.
- [5] Johnson, E.N., et al. *Flight Test Results of Autonomous Fixed-Wing UAV Transitions to and from Stationary Hover*. in *AIAA Guidance, Navigation and Control Conference and Exhibit*. Keystone, Colorado, 2006.
- [6] Frank, A., et al. *Hover, Transition, and Level Flight Control Design for a Single-Propeller Indoor Airplane*. in *AIAA Guidance, Navigation and Control Conference and Exhibit*, 2007.
- [7] Stone, H., et al., Flight Testing of the T-Wing Tail-Sitter Unmanned Air Vehicle. *Journal of Aircraft*, Vol. 45, No. 2, pp. 673-685 2008.
- [8] Stone, H. and G. Clarke. *Optimization of Transition Manoeuvres for a Tail-Sitter Unmanned Air Vehicle (UAV)*. in *Australian International Aerospace Congress*. Canberra, Australia, 2001.
- [9] Kubo, D. and S. Suzuki, Tail-Sitter Vertical Takeoff and Landing Unmanned Aerial Vehicle: Transition Flight Analysis. *Journal of Aircraft*, Vol. 45, No. 1, pp. 292-297 2008.
- [10] Hanley, P., *MultiSurface Aerodynamics*, HanleyInnovations.
- [11] Katz, J., *Low Speed Aerodynamics*: Cambridge University Press. 2001
- [12] McCormick, B.W., *Aerodynamics, Aeronautics, and Flight Mechanics*. Second edition: John Wiley & Sons, Inc. 1994
- [13] Nelson, R.C., *Flight Stability and Automatic Control*. Second edition: The McGraw-Hill Inc. 1998

6 Contact Author Email Address

Adnan Maqsood

adnanmaqsood@gmail.com

The authors confirm that they, and/or their company or organization, hold copyright on all of the original material included in this paper. The authors also confirm that they have obtained permission, from the copyright holder of any third party material included in this paper, to publish it as part of their paper. The authors confirm that they give permission, or have obtained permission from the copyright holder of this paper, for the publication and distribution of this paper as part of the ICAS2010 proceedings or as individual off-prints from the proceedings.